The Location of Diapycnal Mixing and the Meridional Overturning Circulation

JEFFERY R. SCOTT

Program in Atmospheres, Oceans, and Climate, Massachusetts Institute of Technology, Cambridge, Massachusetts

JOCHEM MAROTZKE

School of Ocean and Earth Science, Southampton Oceanography Centre, Southampton, United Kingdom

(Manuscript received 1 May 2001, in final form 14 June 2002)

ABSTRACT

The large-scale consequences of diapycnal mixing location are explored using an idealized three-dimensional model of buoyancy-forced flow in a single hemisphere. Diapycnal mixing is most effective in supporting a strong meridional overturning circulation (MOC) if mixing occurs in regions of strong stratification, that is, in the low-latitude thermocline where diffusion causes strong vertical buoyancy fluxes. Where stratification is weak, such as at high latitudes, diapycnal mixing plays little role in determining MOC strength, consistent with weak diffusive buoyancy fluxes at these latitudes. Boundary mixing is more efficient than interior mixing at driving the MOC; with interior mixing the planetary vorticity constraint inhibits the communication of interior water mass properties and the eastern boundary. Mixing below the thermocline affects the abyssal stratification and upwelling profile but does not contribute significantly to the meridional flow through the thermocline or the ocean's meridional heat transport. The abyssal heat budget is dominated by the downward mass transport of buoyant water versus the spread of denser water tied to the properties of deep convection, with mixing of minor importance. These results are in contrast to the widespread expectation that the observed enhanced abyssal mixing can maintain the MOC; rather, they suggest that enhanced boundary mixing in the thermocline needs to be identified in observations.

1. Introduction

Microstructure and tracer release measurements of diapycnal mixing in the ocean (Polzin et al. 1997; Ledwell et al. 1993, 2000) show that mixing is strongly localized, with diffusivities exceeding 10^{-4} m^2 s^{-1} above rough bottom topography and an order of magnitude less above smooth abyssal plains and in the thermocline. The energy for the diapycnal mixing is thought to come from winds and tides (Munk and Wunsch 1998, hereafter MW) and perhaps geothermal sources (Huang 1999). The strength of the meridional overturning circulation (MOC) in models depends strongly on the choice of the vertical or diapycnal diffusivity (Bryan 1987; Colin de Verdière 1988; Zhang et al. 1999). Hence, diapycnal mixing plays a crucial role in the dynamics of the MOC and of climate because the MOC is an important transport agent of properties relevant for climate.

To date, there have been only a few model studies that specifically examine the dynamical consequences of mixing location. Using an idealized single-hemisphere ocean general circulation model, Cummins et al. (1990, hereafter CHG) parameterized vertical diffusivity as a function of the buoyancy frequency, effectively increasing mixing at depth, particularly below the thermocline. Cummins (1991) examined the results of several additional runs with specified increased mixing below the thermocline. Using a similar model without wind forcing, Marotzke (1997, hereafter M97) imposed mixing only along the boundaries and applied the results as a foundation for a self-contained theory predicting the strength of the MOC. Samelson (1998) applied localized mixing on the eastern boundary to an idealized wind- and buoyancy-forced single hemisphere, planetary geostrophic model. Hasumi and Suginohara (1999) investigated the effects of enhanced mixing over topography in a global model, and Marotzke and Klinger (2000) analyzed the effects of equatorially asymmetric vertical mixing.

Using a single-hemisphere model of the ocean, we explore the effect of spatially varying diapycnal mixing. We juxtapose various extreme scenarios, in that mixing is concentrated entirely at low or high latitudes; at the western boundary, the eastern boundary, or the interior; in or below the thermocline. To our knowledge, the MOC's sensitivity to mixing in so clearly identifiable regimes of the ocean has never been investigated. Our

Corresponding author address: Dr. Jeffery R. Scott, MIT, Room 54-1711, Cambridge, MA 02139.
E-mail: jscott@mit.edu

TABLE 1. Summary of numerical parameters.

Parameter	Value
Basin width, length	60°, 64°
Basin depth	4500 m
Horizontal, vertical viscosity	3.3×10^4 m^2 s^{-1}, 10^{-2} m^2 s^{-1}
Horizontal, isopycnal diffusivity	0 m^2 s^{-1}, 10^3 m^2 s^{-1}
Isopycnal thickness diffusion	10^3 m^2 s^{-1}
Longitude, latitude grid spacing	1.875°, 2°
Number of levels	30
Temperature, salinity restoring timescale	30 days
Time step, momentum	30 min
Time step, tracers	12 h

numerical results lead us to revisit the advective–diffusive balance in the abyss, the deep-ocean heat budget, and how planetary vorticity conservation helps us to understand the MOC. Our configuration is very highly idealized (like M97, we omit wind forcing), but we maintain that the single hemisphere ocean is an appropriate configuration to represent the fundamental dynamics of the MOC.

This paper is organized as follows. In section 2, we briefly describe the ocean model. The ramifications of mixing that is highly localized in the horizontal are examined in section 3. In section 4 we present experiments with depth-dependent diapycnal mixing and examine the deep ocean heat balance and the structure of the overturning cell. We end with a discussion and conclusions in section 5 and section 6, respectively.

2. Model description

We employ the *z*-coordinate, primitive equation model MOM 2 (beta version 2.0), as described in Pacanowski (1996). Default parameters are listed in Table 1. The ocean configuration and forcing are identical to that in M97: the domain is a 60° wide single hemisphere sector, ranging from the equator to 64°, with a constant depth of 4500 m; temperature and salinity are forced using an identical, zonally uniform cosine profile, with peak-to-peak amplitudes of 27°C and 1.5 psu and a 30-day relaxation time constant. Given these identical forcing profiles, the model can be thought of as being forced by buoyancy. Higher-order effects from the nonlinear equation of state are included in the model but are not thought to be important in the results presented here. Therefore, we do not distinguish between temperature and buoyancy. For simplicity, no wind stress is imposed. Our vertical grid spacing ranges from 50 m at the surface to 250 m at the lowest level.

As in M97, diapycnal mixing is imposed in the columns adjacent to the north, south, east, and west sidewalls, and is set to zero elsewhere; this is thought to mimic the effect of enhanced mixing due to a sloping lateral boundary. Diapycnal mixing at the equator is a surrogate for the global integral of mixing throughout the rest of the world's oceans. Although there is evidence of enhanced mixing at the equator (Gregg 1987; Peters et al. 1988) and the dynamics there are unique due to the vanishing of the Coriolis parameter (Gill 1982), our choice of the equator for our southern wall is for practical reasons, as cross-equatorial flow involves complicated dynamics (Marotzke and Klinger 2000) that are beyond the scope of our investigation. To insure that equatorial dynamics were not important in our findings, we spun up a run with the southern boundary mixing moved one grid cell northward (i.e., removed from the equator), with only minor differences resulting.

Mixing is implemented along isopycnals, using the Redi (1982) isoneutral diffusion tensor. We employed the MOM 2 ''full tensor'' option, keeping all terms in the diffusion tensor. In locations of steeply sloping isopycnals, use of this option requires only mild rescaling of the isoneutral diffusion coefficient, as compared to that using the approximate form of the tensor (Griffies et al. 1998; see also Pacanowski 1996). All runs use the Gent–McWilliams (1990) parameterization to represent the effect of mesoscale eddies on isopycnals. Our runs use the (original) advective-flux implementation of the Gent–McWilliams parameterization, as is implemented in MOM 2.

All model runs were integrated to equilibrium, as defined by a basin-averaged surface heat flux of 5×10^{-3} W m^{-2} or less, where practical, and/or when overturning is discernibly within 0.1 Sv (Sv $\equiv 10^6$ m^3 s^{-1}) of its final value. The control run was integrated to equilibrium from an isothermal, motionless ocean. All other experiments were started from the control run or from the equilibrated state of another experiment.

A summary of the numerical experiments is presented in Table 2. Diapycnal mixing does not vary with depth in experiments A–K; in these runs, we aim to understand the effect of mixing location (and degree of localization) in the horizontal. Our control run, experiment A, is very similar to the run described at length in M97. Except for experiments G–K, which employ a background diffusivity of 0.1×10^{-4} m^2 s^{-1} for numerical purposes, diffusivity is set to zero where not prescribed in Table 2. In experiments L–O, diapycnal mixing occurs only along the boundaries, as in our control run, but varies in the vertical, as plotted in Fig. 1.

For computation efficiency, experiments F–K were run at half resolution, that is, $3.75° \times 4°$, 16 vertical levels. In these runs, the diffusivity was adjusted so that the area-integrated diapycnal mixing approximately matched that of the control run. In addition, horizontal viscosity was changed to resolve the Munk boundary layer at the new zonal grid spacing. In section 4, several of the experiments were run with high vertical resolution (90 evenly spaced levels) in order to minimize any adverse numerical effects and to allow for a smoother representation of stratification. In several direct comparisons (not shown), model results did not differ significantly between similarly configured runs at different vertical and/or horizontal resolution.

TABLE 2. Summary of numerical experiments. Mixing in expts A–K is constant with depth.

Expt	Mixing location	κ ($m^2\ s^{-1}$)	
A	N, S, E, W boundaries	10×10^{-4}	
B	Uniform	1.15×10^{-4}	
C	N, S, E, W boundaries, double-width	5×10^{-4}	
D	S boundary; E, W boundaries, 0–36°N	10×10^{-4}	
E	S boundary only	10×10^{-4}	
F	N, S boundaries; 7.5° wide midbasin meridional strip	5×10^{-4}	
G	3.75° × 4° patch along western boundary, various latitudes	80×10^{-4}	
H	3.75° × 4° patch along eastern boundary, various latitudes	80×10^{-4}	
I	3.75° × 4° patch, located at midbasin, various latitudes	80×10^{-4}	
J	Three 3.75° × 4° patches, located along the S boundary	27×10^{-4}	
K	3.75° × 4° patch, centered at 1.875°E, 2°N; rapid restoring	80×10^{-4}	
		Upper κ	Abyssal κ
L	Weak thermocline mixing; N, S, E, W boundaries	see Fig. 1	10×10^{-4}
M	Weak deep mixing; N, S, E, W boundaries	10×10^{-4}	see Fig. 1
N	Strong deep mixing; N, S, E, W boundaries	10×10^{-4}	see Fig. 1
O	Alternate strong deep mixing; N, S, E, W boundaries	10×10^{-4}	see Fig. 1

In order to minimize numerical ''wiggles'' resulting from zero diapycnal mixing in the ocean interior, we employed the flux-corrected transport advection scheme, a nonlinear compromise between upstream and centered differences (Gerdes et al. 1991). In effect, this scheme minimizes numerical noise through the introduction of some diapycnal mixing. We maintain this scheme's supplementary mixing is inconsequential here, based on trial experiments using MOM's other advection schemes and from the results of runs with very weak boundary mixing. The reader is referred to M97 for a discussion of other numerical issues involved with the boundary mixing implementation.

Before proceeding, some additional comments are in order regarding boundary layers, several of which cannot be resolved by our model. Reasonable treatment of western boundary currents is possible, albeit using an unrealistic viscosity coefficient due to our coarse grid spacing. As noted in Huck et al. (1999), however, the parameterization of the lateral boundary conditions can influence the large-scale circulation. Here, two notable features of our solution—narrow upwelling along the eastern and western boundary and deep downwelling in the northeast corner—are enhanced by (or perhaps even caused by) by our use of no-slip side boundaries with Laplacian momentum dissipation. The so-called Veronis effect (Veronis 1975) whereby a Cartesian implementation of diffusion is thought to effect spurious horizontal mixing in the western boundary, producing upwelling, does not occur here given our use of the isopycnal mixing scheme. Huck et al. (1999) argue that the lateral boundary parameterization induces upwelling, which in turn causes the Veronis effect rather than vice versa. Huck et al. also showed that the model solution differs when a linear frictional closure scheme for tangential velocity is introduced into the vorticity equation, such as proposed in Winton (1993). It is not clear which boundary parameterization is superior for the purpose of modeling the real ocean, given a lack of observational evidence and our limited understanding of eddy dissipation processes (see Huck et al. for a more complete discussion). For practical reasons, we must assume that the results described here reflect upon the fundamental thermodynamics of the model's large-scale circulation rather than local features specific to the model implementation. The effect of other omissions, particularly the absence of wind stresses and topography, is addressed in our discussion section.

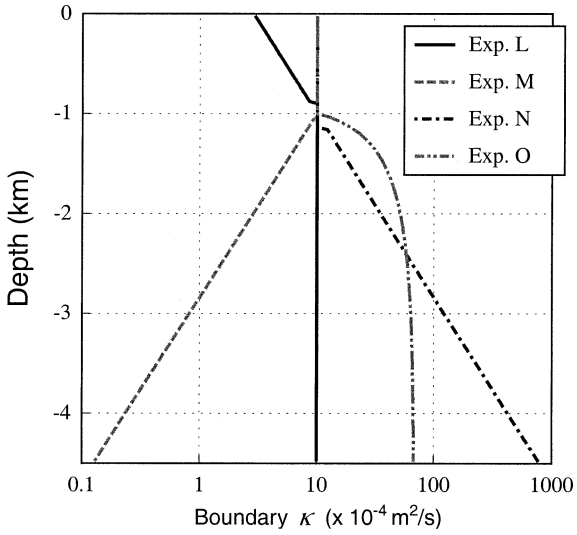

FIG. 1. Vertical profile of boundary diapycnal diffusivity for weak thermocline mixing (expt L), weak deep mixing (expt M), and our two strong deep mixing experiments (expts N and O).

3. Horizontal location of mixing

a. Boundary versus uniform mixing

In the model runs of M97, boundary flows set up an east–west temperature gradient that, through thermal wind balance, supports a MOC. We have repeated the M97 boundary mixing control run here (expt A); minor

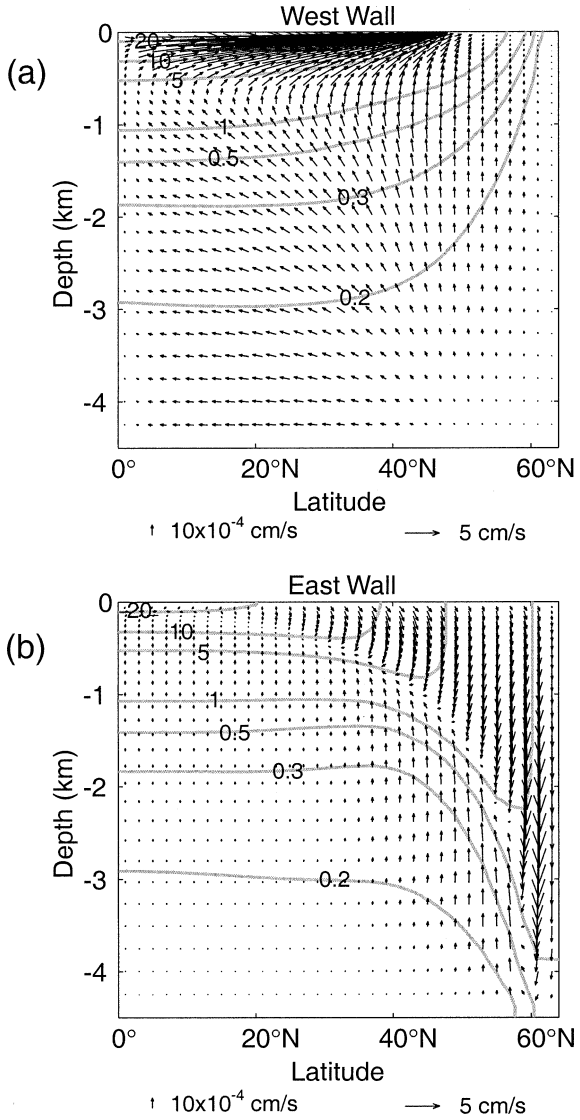

FIG. 2. Boundary mixing run (expt A), $\kappa = 10 \times 10^{-4}$ m^2 s^{-1}. (a) Temperature (contour levels as indicated) and flow along the western wall; (b) temperature and flow along the eastern wall. Vertical and horizontal velocity scales are shown for reference.

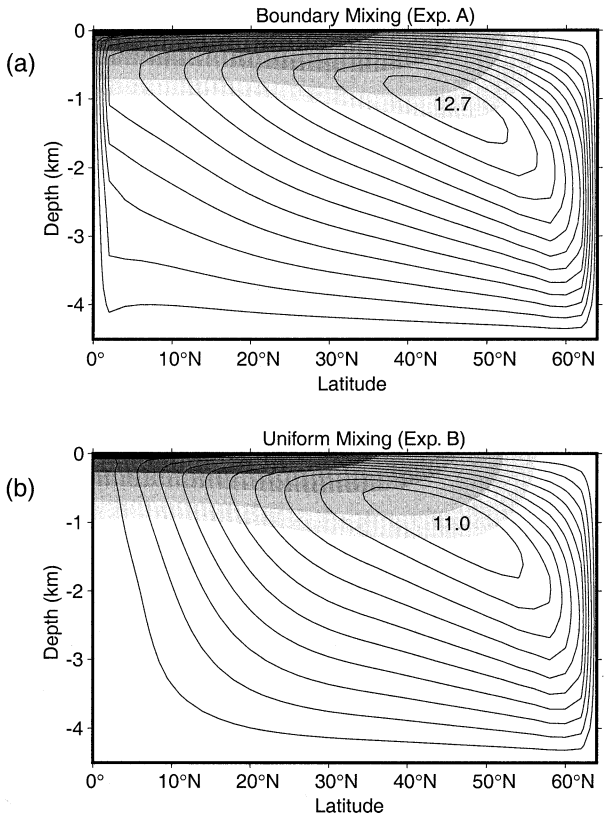

FIG. 3. Meridional overturning streamfunction (contours) and zonally averaged temperature (shading) for (a) boundary mixing run (expt A), $\kappa = 10 \times 10^{-4}$ m^2 s^{-1} and (b) uniform mixing run (expt B), $\kappa = 1.15 \times 10^{-4}$ m^2 s^{-1}. In this and all subsequent plots of overturning streamfunction and zonally averaged temperature, overturning contours interval is 1 Sv; isotherms are at 0.05, 0.1, 0.2, 0.4, and 0.8 $\times$ ΔT ($\Delta T = 27$°C); flow is oriented clockwise around overturning maximum.

differences are due to our use of improved resolution and the isopycnal mixing scheme. As in M97, upwelling occurs all along the west wall (Fig. 2a), advecting dense deep waters into the thermocline. On the east wall (Fig. 2b), however, the vertical flow pattern is more complicated. Upwelling occurs at depth, but surface flow downwells to increasing depths at high latitudes. Since the downwelling surface water is relatively warm, the eastern wall is less dense than the western wall, providing the necessary shear for zonally integrated southward flow at depth and northward flow in the upper ocean.

The meridional mass transport streamfunction for the control run is shown in Fig. 3a. Over 5 Sv, or almost half of the net mass transport, upwells adjacent to the equator where diapycnal mixing is concentrated. To examine the effect of the boundary mixing parameterization, we equilibrated a run with uniform diapycnal mixing diffusivity of 1.15×10^{-4} m^2 s^{-1} (expt B), that is, that which produces an area-integrated diffusivity equivalent to that of the control run. Detailed analyses of a similarly configured uniform mixing run, albeit with cruder numerics, are presented in Colin de Verdière (1988). Superficially, the MOC of the uniform mixing run (Fig. 3b) shows little difference from the boundary mixing run. The maximum of the overturning stream function is 1.7 Sv less in the uniform case, reducing the ocean's northward peak heat transport from 0.55 to 0.47 PW (PW = 10^{15} watts). With mixing spread out more evenly over the low latitudes, a much smaller proportion of the upward mass transport flows adjacent to the southern boundary. As would be suggested by our discussion in the previous section, strong vertical flows are present along the east and west boundaries, even in the uniform mixing case. Some of this flow recirculates zonally without contributing to the MOC [see Bryan (1987) for a diagnosis of the meridionally averaged circulation and

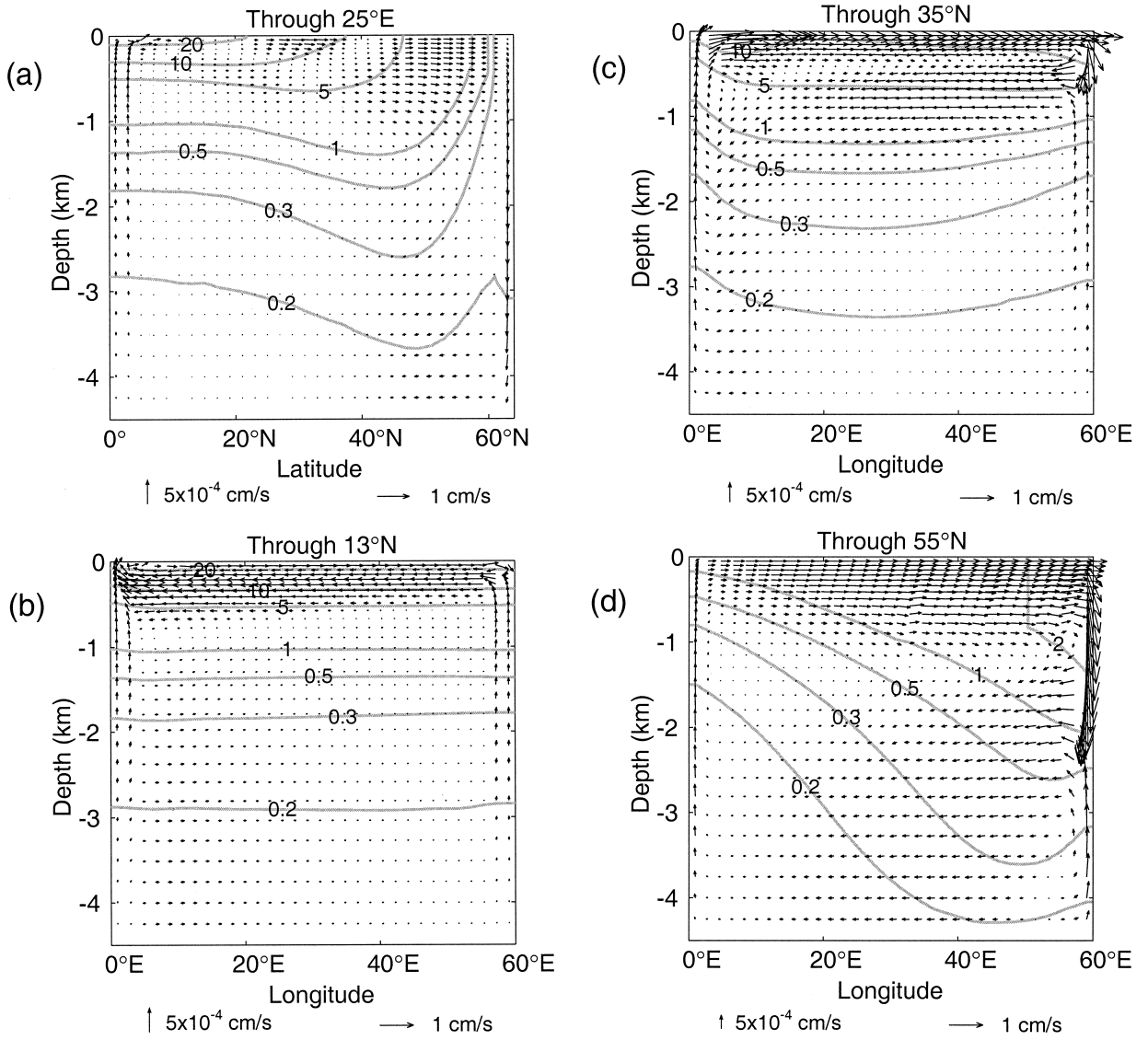

FIG. 4. Two-column boundary mixing run (expt C), $\kappa = 5 \times 10^{-4}$ m^2 s^{-1}. (a) Temperature and flow along the meridional plane through 25°E; (b) temperature and flow along the zonal plane through 13°N; (c) temperature and flow along the zonal plane through 35°N; (d) temperature and flow along the zonal plane through 55°N.

its scaling behavior with vertical diffusivity], while some of western upwelling moves northward along isopycnals. As such, it is not immediately clear what component of these boundary flows is diapycnal.

To determine which boundary flows are directly induced by diapycnal mixing, presumably through advective–diffusive balance, and which are a largely a consequence of lateral boundaries, we ran an experiment where we expanded the region of diapycnal mixing to two boundary grid columns around the model sidewalls (expt C). For consistency, we decreased the magnitude of κ by 50%. In addition, we resolved the Munk boundary layer across two zonal grid points. As with the uniform mixing run, imposing mixing away from the boundaries results in a decreased maximum in the overturning streamfunction (not shown), although the reduction here is only 0.3 Sv. Near the equator, both meridional grid columns with mixing show strong upwelling, as shown in Fig. 4a, while interior flows are very weak in the meridional–vertical plane. In low latitudes, there are two columns of strong upwelling at both the eastern and western boundaries (Fig. 4b). This result is consistent with Colin de Verdière (1988), who diagnosed that the primary balance in low latitudes was between diffusive heating and cold upwelling. Similarly, Samelson (1998) observed strong upwelling in low latitudes along the eastern boundary, where his mixing was concentrated. Although some upwelling is evident in two columns at the boundaries at midlatitudes (Fig. 4c), the magnitude is much larger in the columns di-

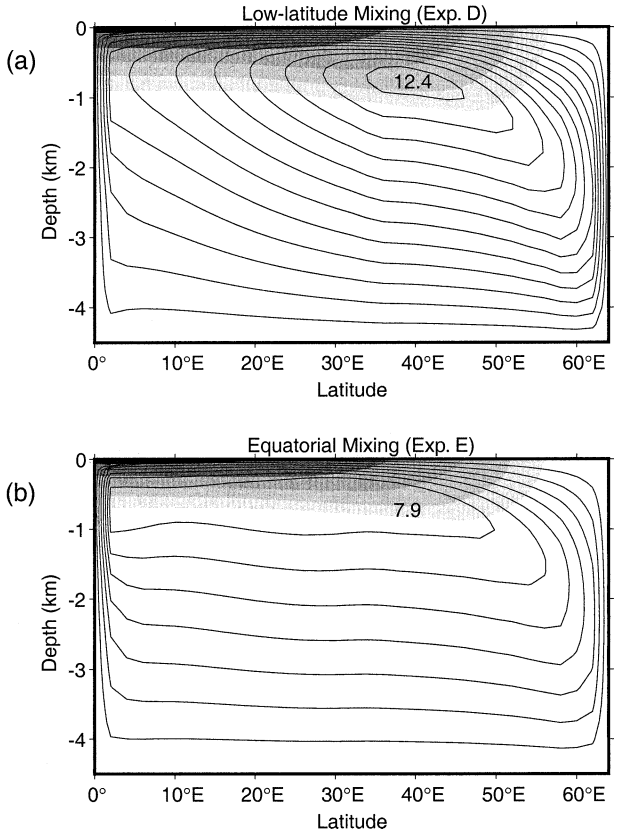

FIG. 5. Meridional overturning streamfunction (contours) and zonally averaged temperature (shading) for (a) low-latitude boundary mixing run (expt D), $\kappa = 10 \times 10^{-4}$ m^2 s^{-1} between 0 and 36° lat, otherwise diffusivity is set to zero; and (b) equatorial mixing run (expt E), $\kappa = 10 \times 10^{-4}$ m^2 s^{-1} between 0° and 2° lat, otherwise diffusivity is set to zero.

rectly adjacent to the boundary. At high latitudes, nearly all upwelling in the west occurs adjacent to the boundary, as shown in Fig. 4d; in the east, some upwelling is apparent in both columns, although there is a large disparity in the velocities, as in the midlatitude section. These results suggest that the mixing at low latitudes, in effect, drives local upwelling through vertical advective–diffusive balance. At middle and high latitudes, where stratification is generally weak, a large percentage of the vertical flow at the east–west boundaries is the result of mass convergence and subsequently a component of the vertical flow is oriented along isopycnals.

b. Low-latitude mixing and midbasin mixing

Motivated by these results, we wish to examine whether mid- and high-latitude mixing plays any significant role in the dynamics of the modeled MOC. Figure 5a shows the meridional overturning streamfunction given boundary mixing from the equator to 36°N, with no diapycnal mixing to the north (expt D). As compared with the control run (Fig. 3a), the center of the overturning cell is several hundred meters higher in the water column, but there are no apparent differences in the zonally averaged temperature profile and the difference in overturning maximum is only 0.3 Sv. In addition, there are only slight differences in the east and west wall boundary layer flows in mid and high latitudes (not shown).

If we further concentrate all mixing at the equator (expt E), the maximum in overturning drops by 38% to 7.9 Sv (Fig. 5b), as we have reduced the area of mixing from the previous low-latitude mixing experiment by 50%. Thus, the subtropical mixing on the east and west walls does contribute in driving the MOC. This result is consistent with significant upwelling into the thermocline along these latitudes, as suggested by the overturning pattern in runs that include mixing in the subtropics (e.g., Figs. 3a and 5a).

As mentioned in the introduction, the results from recent microstructure measurements suggest elevated mixing in the water column above the Mid-Atlantic Ridge. To this end, we ran a variation on our control run where we moved the mixing on the eastern and western boundaries to two adjacent meridional strips down the middle of the ocean, preserving the area-integrated diffusivity (expt F). This experiment produced a similar pattern of overturning as the control run (not shown). However, consistent with other runs that imposed interior mixing, the overturning cell was slightly weaker, comparable in magnitude with the uniform mixing experiment.

c. Highly localized mixing

The previous results suggest that the MOC cell depends critically on the meridional distribution of diapycnal mixing, with the zonal distribution being less important. In this subsection we take these experiments to their logical extreme, localizing mixing to a single grid column. Our motivation here is to facilitate a more detailed examination of the dynamical significance of interior versus boundary mixing (we do not claim that these extreme scenarios are representative of the real ocean). The diapycnal diffusivity in the ''mixing column'' was chosen so that the area-weighted diffusivity in latitudes 0°–36°N matched that of the control run. However, to control numerical difficulties we also added a background diffusivity of 0.1×10^{-4} m^2 s^{-1}, the value typically assumed for the ''pelagic diffusivity'' (MW). In a run with uniform diffusivity set at this background value, the overturning streamfunction maximum is 2.3 Sv, considerably weaker than that observed in this set of experiments.

We equilibrated runs with the mixing column at three zonal locations—the western boundary (expt G), at the eastern boundary (expt H), and at midbasin (expt I)—and at latitudes ranging from 2°N to 50°N. Consistent with the previous results, nearly all the MOC's upwelling occurs where mixing is located. Figures 6a–c show the temperature and flow in the bottom layer, ther-

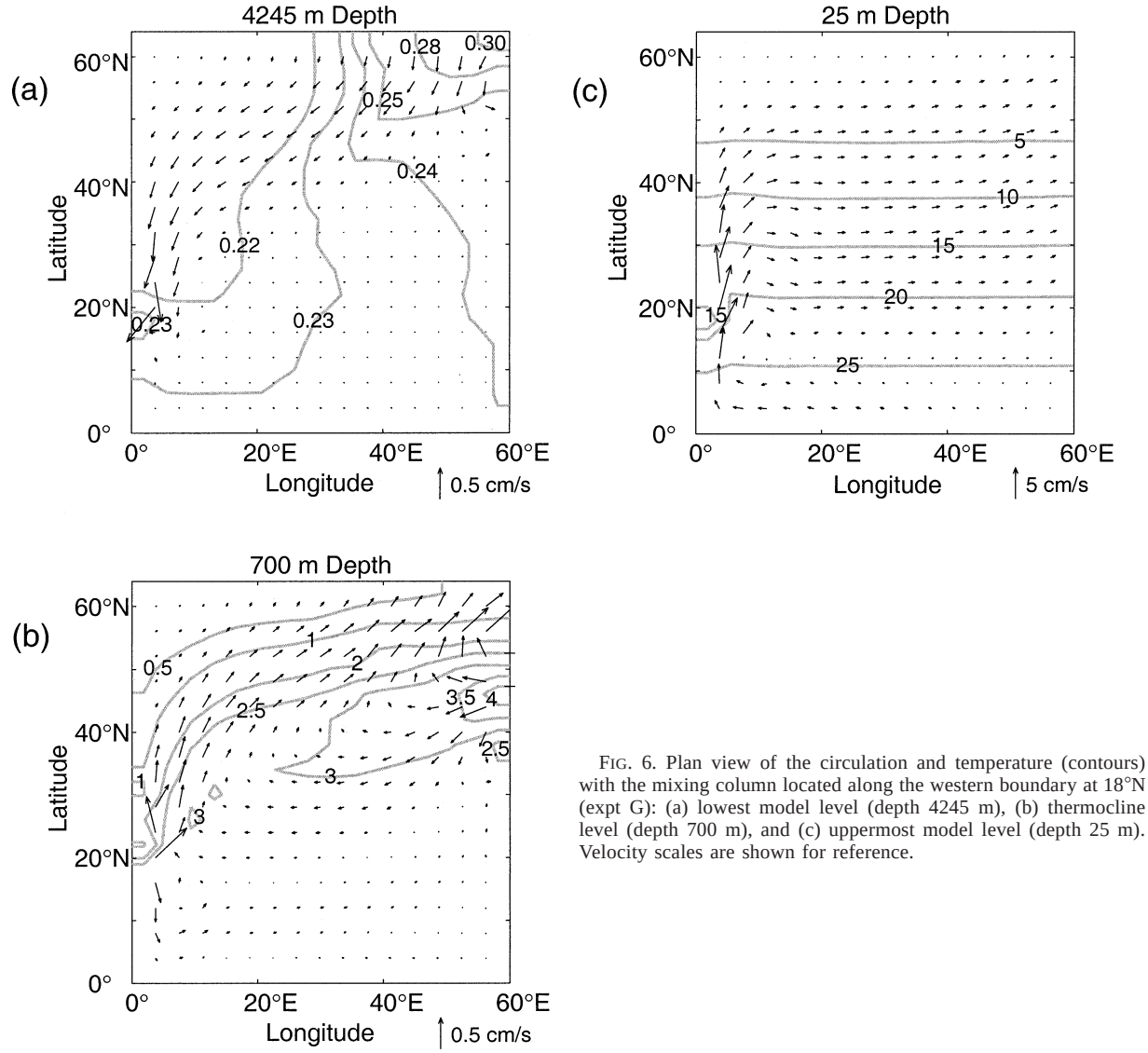

FIG. 6. Plan view of the circulation and temperature (contours) with the mixing column located along the western boundary at 18°N (expt G): (a) lowest model level (depth 4245 m), (b) thermocline level (depth 700 m), and (c) uppermost model level (depth 25 m). Velocity scales are shown for reference.

mocline, and surface layer, respectively, for a mixing column located at 18°N along the western boundary. The plots show deep convergence and upper level divergence in the mixing column; note that in this configuration, the deep western boundary current is effectively short-circuited by the upwelling in the mixing column. Figures 7 and 8 show a similar low-level convergence and upper-level divergence in the mixing column when it is situated at the eastern boundary or ocean interior, respectively.

Figure 9 shows the maximum in overturning streamfunction for the three series as a function of the mixing column latitude. As the mixing location moves farther north, the MOC decreases in intensity, most noticeably when the mixing is located in the interior. Conversely, the circulation remains strongest when the mixing is located on the eastern boundary.

As a starting point in explaining Fig. 9, let us examine the scaling behavior of the MOC. A simple predictive scaling relationship for the overturning circulation was first presented by Bryan and Cox (1967) (see also Welander 1971). The following balances are employed:

vertical advective–diffusive balance:

$$W \sim \frac{\kappa}{D} \tag{1}$$

continuity:

$$\frac{V}{\Delta x} \sim \frac{W}{D} \tag{2}$$

thermal wind balance:

$$\frac{V}{D} \sim \frac{g\alpha}{f}\frac{\Delta T}{L_x}, \tag{3}$$

where V and W are horizontal and vertical velocity

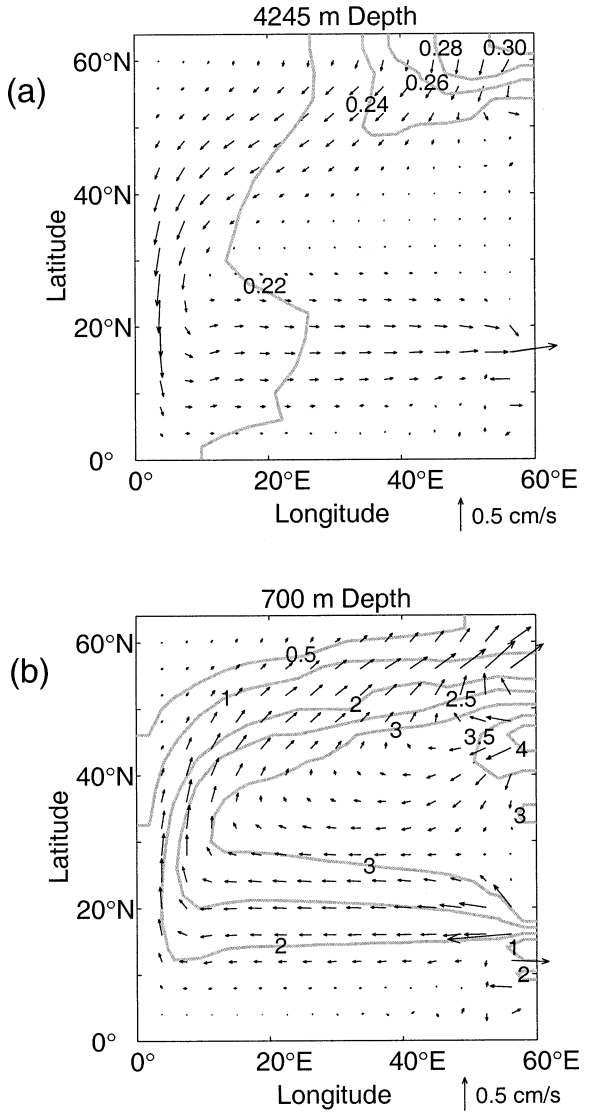

FIG. 7. Plan view of the circulation and temperature (contours) with the mixing column located along the eastern boundary at 18°N (expt H): (a) lowest model level (depth 4245 m) and (b) thermocline level (depth 700 m).

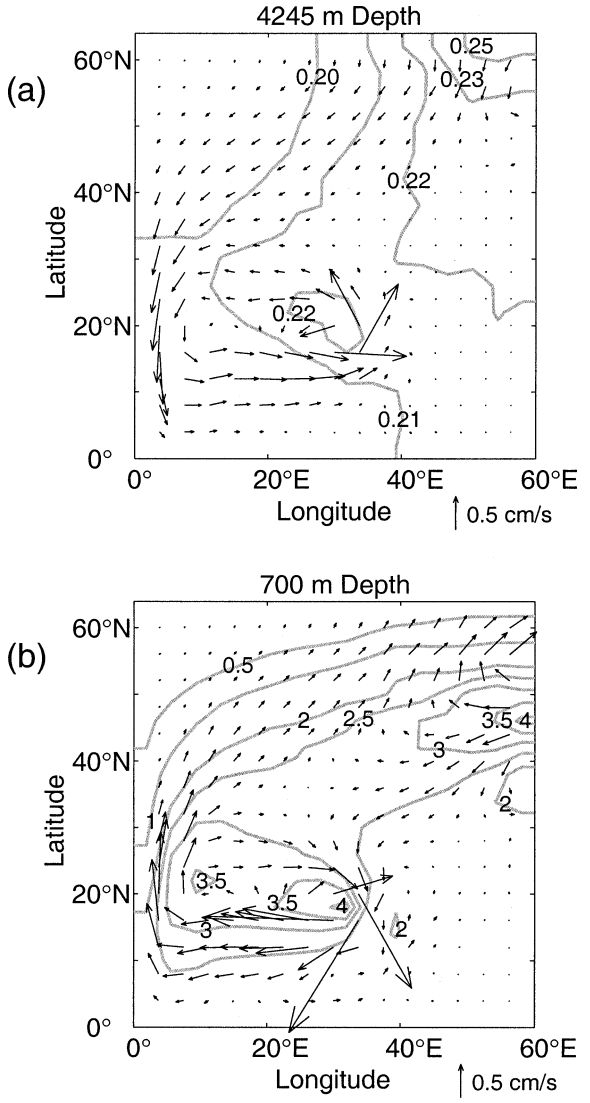

FIG. 8. Plan view of the circulation and temperature (contours) with the mixing column located at midbasin (32°E) and 18°N (expt I): (a) lowest model level (depth 4245 m) and (b) thermocline level (depth 700 m).

scales, respectively, D is a vertical length scale [albeit somewhat ambiguously defined; see Scott (2000) for a more complete discussion of how this contributes to problems in using (1)–(3) to predict scaling behavior], and κ is a vertical (or diapycnal) diffusivity. Traditionally, ΔT is taken as the equator-to-pole temperature gradient, and Δx and L_x are taken to be identical, a horizontal length scale. Marotzke (1997) and Park and Bryan (2000) suggest that the equator-to-pole temperature gradient scales as the east–west temperature gradient; it is the latter that is directly related to the meridional velocity and thus meridional overturning. Here, we consider Δx as a horizontal length scale over which upwelling occurs, corresponding to the generation of horizontal velocity by convergence of vertical velocity; L_x is a horizontal length scale over which the east–west temperature gradient occurs (presumably at midlatitudes, near the maximum in overturning). As noted in M97, the relevant east–west temperature gradient occurs across the western boundary current.

By eliminating W from (1) and (2) and eliminating V using (3), the following scales for V and D are obtained:

$$V \sim \left[\frac{\kappa \Delta x (g\alpha \Delta T)^2}{f^2 L_x^2}\right]^{1/3}, \qquad D \sim \left(\frac{\kappa \Delta x f L_x}{g\alpha \Delta T}\right)^{1/3}. \quad (4)$$

The meridional overturning Ψ can in turn be estimated as $\sim VDL$, suggesting a $(\kappa \Delta x)^{2/3}$ dependence. In other words, both the depth scale and the maximum of overturning scale as a function of the area-integrated mixing

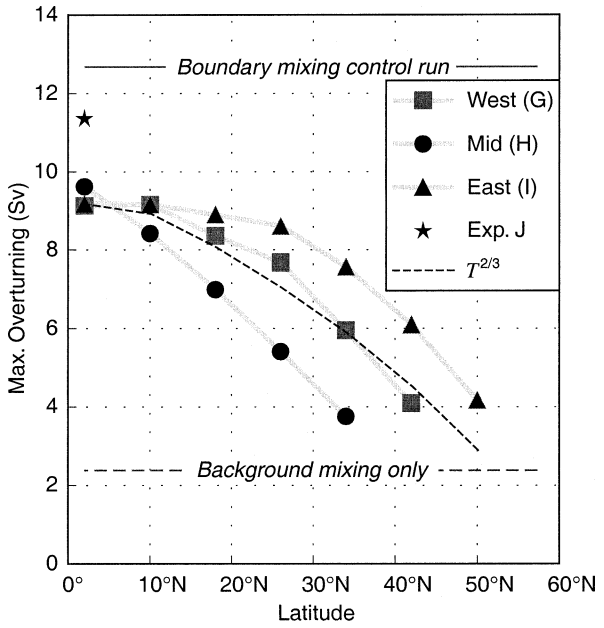

FIG. 9. Maximum in overturning streamfunction for highly localized mixing expts G, H, I, and J. The abscissa reflects the meridional location of the mixing column with $\kappa = 160 \times 10^{-4}$ m^2 s^{-1}, otherwise the diffusivity is set to a background value of $\kappa = 0.1 \times 10^{-4}$ m^2 s^{-1} (these runs were done using 3.75° × 4° resolution). The three series show results for different zonal locations of the mixing column, i.e., adjacent to the western wall, adjacent to the eastern wall and at midbasin (expts G, H, and I, respectively). The solid star indicates the result when mixing is equally divided into three equatorial columns at these zonal locations (expt J).

(see also Samelson 1998), consistent with our results here (Δx encapsulates both the meridional scale and the zonal scale of the mixing area). Note that neither the basin width nor the basin's meridional scale (i.e., the distance between the tropical mixing and high latitudes) enters the scaling relationship. This was confirmed in a test run where we decreased the zonal width of the basin (with mixing in a single column) and a second test run with ''tropical'' mixing (and tropical temperatures) located at 20°N rather than along the equator. In both these test runs, the maximum in overturning was little changed. Thus, changes in either zonal or meridional length scales associated with our localized mixing run parameterization do not explain the behavior exhibited in Fig. 9.

Upon further scrutiny, there are three competing effects that are important here, which we address separately. Although the first effect is captured in (4), the latter two involve dynamics that the scaling relation is incapable of representing.

1) SURFACE BOUNDARY CONDITIONS

An examination of the surface temperature immediately suggests why all of the highly localized mixing experiments plotted in Fig. 9 produce weaker overturning than the control mixing run: where upwelling occurs, the surface is quite cold, approximately 10°C colder than neighboring grid points, so the diffusion of heat into the thermocline is far less efficient than in the less localized mixing runs [i.e., decreasing ΔT in (4)]. In the midbasin, equatorial mixing run the surface anomaly in temperature is about 1°C less than when the mixing is at the equatorial western or eastern boundary, consistent with its slightly stronger overturning circulation. To further test this hypothesis, we ran two additional experiments. First, we divided the mixing evenly between three equatorial columns located in the west, east, and midbasin (expt J). As indicated by the solid star in Fig. 9, the overturning circulation was 2 Sv stronger, consistent with the steady-state temperature at these three points being much closer to the restoring profile than in the single column mixing runs. Second, we changed the surface restoring time constant from 30 days to 2 days (expt K). With the mixing column located in the southwest corner, the circulation increased to match that of the control run (but since the mixing column experiments employ the weak pelagic background mixing, we caution that the nearly exact agreement is not quite as ''clean'' as this result might suggest).

As the mixing column moves north, the surface restoring temperature decreases, providing a simple explanation for the noted decrease in overturning strength. The dashed line in Fig. 9 is a plot of the observed model surface temperature for the eastern mixing series as a function of mixing column latitude, taken to the two-thirds power and then normalized to coincide with the maximum overturning at the equator (the decrease in surface temperature with latitude is similar for the western and midbasin mixing series). This power law is chosen as the approximate functional dependence of maximum overturning on the high to low latitude temperature difference [Scott 2000; note this differs somewhat from that predicted by (4)]. We see that with western boundary mixing, the fall off with latitude is close to that predicted by the decrease in surface temperature. However, at high latitudes the eastern boundary mixing series is stronger than predicted while the interior mixing series is weaker, suggesting that additional factors play a role in determining the overturning strength as the mixing latitude is varied.

2) INTERIOR VERSUS BOUNDARY MIXING

Dynamical considerations suggest a different behavior of the interior localized mixing runs, compared to the boundary mixing runs; in this section, we go through this—fairly involved—chain of reasoning. In all cases, the mixing causes upwelling at the mixing locations; this upwelling must be fed by converging horizontal flow, ultimately by southward flow emanating from the deep-sinking locations. But the upwelling and meridional flow are also linked dynamically: Assuming a geostrophic ocean interior, the planetary geostrophic vorticity equation

$$\beta v = f\frac{\partial w}{\partial z} \tag{5}$$

implies that any deep convergence (producing upwelling and hence vortex stretching) must be balanced by northward flow. This connection exists for upwelling in the basin interior but not for upwelling at the side walls, where (5) would not be expected to be a good approximation (Stommel and Arons 1960; Spall 2000). The following considerations apply in a scenario that has the same amount of water upwelling in the interior as would upwell at the same latitude but at a wall.

When mixing is highly localized in the ocean interior, the magnitude of $\partial w/\partial z$ is quite large, producing a strong recirculation in both the abyss and in the thermocline, as shown in Figs. 8a and 8b, respectively [see Pedlosky (1996, 405–409) for an analytical treatment of a localized abyssal sink; see also Spall (2000)]. At both depths, the recirculation is associated with a warm anomaly extending westward from the mixing column. In the thermocline, vortex compression produces a recirculation of opposite sense as the flow at depth, consistent with anomalous warmth above the level of no motion. The upper level recirculation is supported geostrophically by the diffusive heat flux ''trapped'' between the mixing column and the western wall. The westward propagation of the anomaly is due to the β effect, the dynamics of which are described in Stommel (1982) for a geothermally driven warm anomaly. Notice that the anomaly is not advected to the east wall, where it could instead support the MOC.

To support a given rate of upwelling at different latitudes, the intensity of the warm anomaly scales as f^2/β, from (5) and the requirement that the anomaly be in thermal wind balance with v at the upwelling location. As f^2/β increases monotonically with latitude, an increasingly strong anomaly would be required, which however cannot be created. Thus, only weaker upwelling can be supported, and the difference between the midbasin and boundary mixing series plotted in Fig. 9 grows sharply with mixing latitude.

3) Eastern versus western boundary mixing

From thermal wind considerations alone one might expect diffusive warming on the eastern boundary to support a strong MOC, whereas it is not clear how warming on the western boundary can support even a weak MOC. In reality, the dynamics are more complicated than suggested by this argument. If the low-latitude thermocline is heated diffusively, whether in the east or west, a meridional temperature gradient exists at midlatitudes in concert with strong zonal flow and subsequent downwelling on the eastern boundary. This downwelling is the main mechanism that warms the eastern boundary, thus helping to provide the shear necessary for the MOC. Note that the high-latitude flow and temperature structure is similar in the thermocline whether mixing is located in the west (Fig. 6b), east (Fig. 7b), or midbasin (Fig. 8b).

Instead, it is at lower latitudes where the distinction between the eastern and western localized mixing runs is more apparent. Notice, first, that the MOC is confined to the north of the mixing latitude. When mixing occurs on the eastern wall, the deep western boundary current turns and flows eastward across the basin (Fig. 7a) at the latitude of the mixing column. The low-level convergence into the eastern boundary causes upwelling from the abyss and divergence in the thermocline, producing opposite (westward) flow across the basin (Fig. 7b). In order to support this flow geostrophically, it must be colder in the Tropics, as this depth is above the level of no motion. It must remain warm northward of the mixing latitude, or else geostrophic eastward flow would occur; note the large tongue of water with temperature greater than 3°C.

In contrast, when mixing occurs only at the western boundary, significant zonal flow does not occur at low latitudes (Fig. 6b). At this depth the temperature in the Tropics is a full degree higher than with localized eastern mixing, yielding the result that the tropical thermocline is actually deeper in the run with smaller overturning. This may seem surprising, as it has long been assumed that the meridional overturning scales as the thermocline depth, but the caveat here is that the overturning does not extend to these tropical latitudes.

Building on these differences, we now address why the aforementioned disparity in the eastern and western mixing series increases with mixing latitude (Fig. 9). As the mixing column moves northward and f increases, weaker flow is in thermal wind balance with a similar density gradient. With mixing on the western boundary, it becomes increasingly difficult for geostrophic currents to advect the diffusive warming over to the eastern boundary at midlatitudes. Conversely, as mixing on the eastern boundary moves northward it approaches the site of warm water injection, forming a cohesive warm anomaly that supports the dominant circulation—an anticyclonic gyre above a deep cyclonic gyre—even as the mixing column moves quite far to the north.

Finally, we return to our comparison of the boundary mixing control run with the uniform mixing run. As with localized interior mixing, uniform mixing leads to horizontal recirculation (as evidenced by stronger western boundary currents) supported by a warm anomaly (or, equivalently, less anomalous cooling) on the western side of the basin interior, consistent with the modest reduction in the overturning maximum.

The wavelike pattern in Fig. 6b along the western boundary to the north of the mixing latitude is, to a lesser extent, present to the south of the mixing latitude when the mixing is located on the east (as shown in Fig. 7b). Since this behavior does not ostensibly affect the conclusions presented here, we did not investigate further whether we were, in fact, observing stationary Rossby waves or spurious ''wiggles'' related to contrast

between the intense local and weak background diffusivities.

The maximum in meridional heat flux also decreases sharply as the mixing column moves northward (not shown), as might be expected given the decrease in overturning strength. However, there is less disparity in the three series as compared to that shown in Fig. 9. Although the overturning is weaker with midbasin mixing, a small ''eddy'' contribution to the meridional heat flux (i.e., due to deviations from the zonal mean) is positive at the latitude of maximum flux, whereas the contribution is negative for both other series, particularly with mixing located on the eastern boundary. We also note that the latitude of maximum meridional heat flux, approximately 20°N for our standard boundary mixing run, moves to the north if the mixing column is moved northward of this location. The reader is referred to Samelson (1998) for a more in-depth discussion of the effect of localized mixing on the meridional heat transport.

4. Depth-dependent mixing

a. Numerical results

The preceding section investigated the response of the MOC to the horizontal location of mixing. Now we turn to the dependence on where in depth mixing occurs. We performed four additional runs, with vertical profiles of mixing given in Fig. 1: a weak thermocline mixing case (expt L), with our standard boundary mixing below 1000 m and exponentially decaying boundary diffusivity toward the surface; a weak deep mixing case (expt M), retaining the standard boundary mixing in the top 1000 m but exponentially decreasing the boundary diffusivity below; a strong deep mixing case (expt N) where the boundary mixing is exponentially increased below 1000 m; and a second strong deep mixing scenario (expt O), with a sharp increase below the thermocline but nearly constant diffusivity in the abyss. Note that our choice of 1000 m for the thermocline depth was determined a posteriori, based on results from the control experiment.

When mixing is decreased in the thermocline (expt L), the thermocline depth decreases and the maximum in overturning strength is reduced to 7.0 Sv (not shown). The model's meridional heat flux is also considerably weaker. The ramifications of this result, particularly in the context of thermodynamic considerations, are considered in our discussion section.

The overturning streamfunction for the weak deep mixing case (expt M) is shown in Fig. 10a. The maximum in overturning strength decreases by only 0.2 Sv as compared with the control run (Fig. 3a), and there is no apparent change in the zonally averaged thermocline. However, upwelling at depth along the equator is much weaker so that upwelling through the abyss is more evenly distributed meridionally rather than concentrated where mixing (albeit weak) is parameterized.

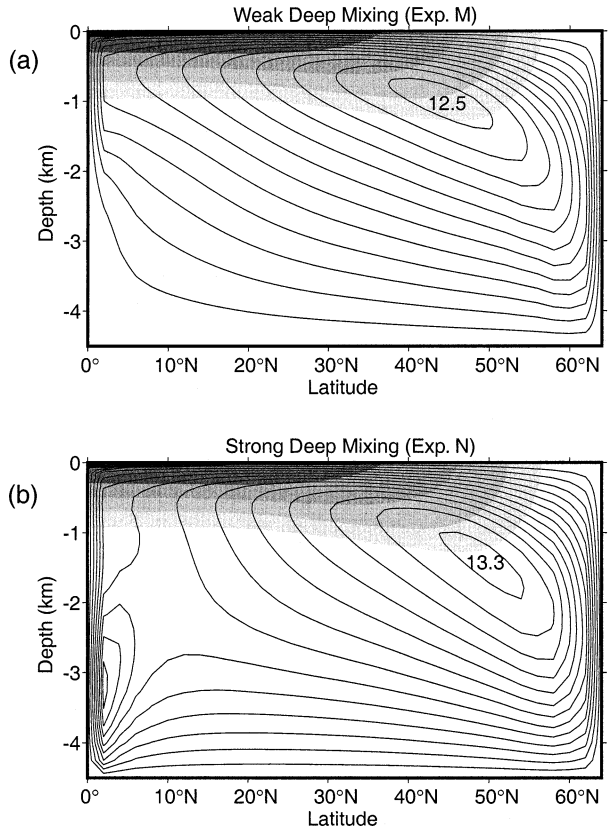

FIG. 10. Meridional overturning streamfunction (contours) and zonally averaged temperature (shading) for (a) weak deep mixing (expt M) and (b) strong deep mixing (expt N).

In contrast, the exponentially increasing strong deep mixing run (expt N) gives rise to vigorous upwelling at the equator (Fig. 10b), producing a deep secondary maximum in overturning. Approximately 3 Sv upwells near the equator at depth but subsequently downwells in the subtropics. In as much as the equatorial upwelling through the thermocline here is similar to that in the control and weak deep mixing runs, the overturning maximum is increased by less than 1 Sv. The maximum meridional heat transport in the three runs varies by less than 0.01 PW, again suggesting that any changes in the deep circulation do not affect the flow through the surface layer or thermocline.

Our experiment N is similar to those discussed in CHG, although their parameterization of vertical diffusivity as a function of N^{-1} also implies increased mixing with depth within the thermocline. Cummins (1991) performed several experiments with varied mixing at depth, although his profiles of vertical diffusivity exhibited a rather sharp increase at the base of the thermocline, in contrast to our slow exponential increase in our experiment N. In both CHG and Cummins, the increase in deep abyssal diffusivity was an order of mag-

nitude less than that here. Despite these differences in the implementation of deep mixing, all results concur that the meridional heat flux is not sensitive to deep mixing. In contrast with our study, however, the CHG and Cummins results suggest that the maximum in overturning streamfunction can, in fact, be quite sensitive to deep mixing. To examine this disparity, experiment O has a more sharply increased diffusivity near the base of the thermocline (i.e., similar to the Cummins profile, although our increase was somewhat less steep than that indicated by his Fig. 1). In experiment O, our model's MOC exhibited a more significant increase than in experiment N, again with only a minor change in the meridional heat flux. Nevertheless, our maximum in overturning is less sensitive to deep mixing than in CHG and Cummins. Note that our secondary meridional cell is much stronger than that shown in CHG's Fig. 4a, which we attribute to our boundary mixing implementation. With strong equatorial mixing the secondary cell is quite distant from the high-latitude maximum in overturning, allowing for less superposition of the deep circulation and the large-scale buoyancy-driven overturning. It is also possible that their use of a Cartesian mixing scheme contributes to their sensitivity. For example, the maximum of the MOC is deeper in M97's Cartesian boundary mixing run than in our isopycnal mixing run. With a deeper maximum, more superposition with this secondary deep circulation is possible.

b. Abyssal heat balance

That deep diffusivity plays so little role in setting the overall strength of the MOC is surprising, given the importance that has been attributed to abyssal mixing (Munk 1966; Polzin et al. 1997; MW). To understand how the steady-state dynamics are affected by deep mixing, it is useful to more carefully examine the model's deep stratification and abyssal heat budget. Figure 11a shows a comparison of $T(z) - T(-H)$ with $\partial T/\partial z$ for our ''control'' boundary mixing run. Both quantities are shown as measured at the western equatorial boundary (the behavior is qualitatively similar throughout the Tropics). It is readily shown that in the Tropics, where upwelling is ''induced'' by prescribed mixing, the model's stratification and w are consistent with one-dimensional advective–diffusive balance (see also Samelson 1998), with the surface and bottom temperatures as boundary conditions; in fact, the resulting solution is nearly an exact match with the model's temperature profile. Thus, horizontal advection (i.e., due to sloping isopycnals) does not play any significant role in setting stratification in the tropics, except at the bottom boundary where $w(z)$ vanishes.

The abyssal heat budget as illustrated in Fig. 12. Downwelling water in the northeast corner is relatively buoyant (Marotzke and Scott 1999), producing a warm anomaly with associated cyclonic flow in the deep ocean. Some of the flow immediately turns and upwells

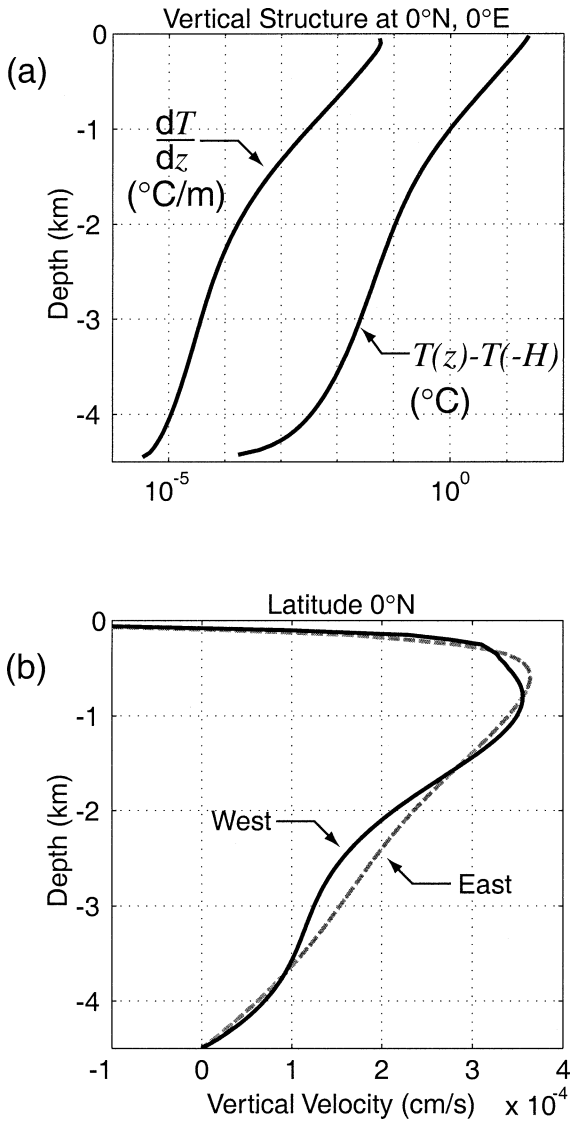

FIG. 11. (a) Vertical potential temperature structure in low latitudes along the boundary, as exemplified by this plot of $T(z) - T(-H)$ and dT/dz at 0°E, 0°N (from expt A). (b) Vertical velocity adjacent to the equatorial boundary, as shown for the westmost and eastmost grid points.

along the eastern boundary; as illustrated in Fig. 2b, the strongest upwelling occurs adjacent to downwelling, tending to cool the eastern boundary higher in the water column (note the cold anomaly between 30°–40°N on the eastern boundary in Figs. 6b, 7b, and 8b). Most of the flow however continues westward across the basin, passing near deep convection. In these model runs deep convection reaches the bottom in the northwestern corner, which is relatively stagnant (and therefore cold) because the upper western boundary current separates from the ''coast'' between 40°N and 50°N. Deep convection is not a source of deep mass flux, so there is no divergence of flow to spread the water mass properties of the convectively mixed column. Because the

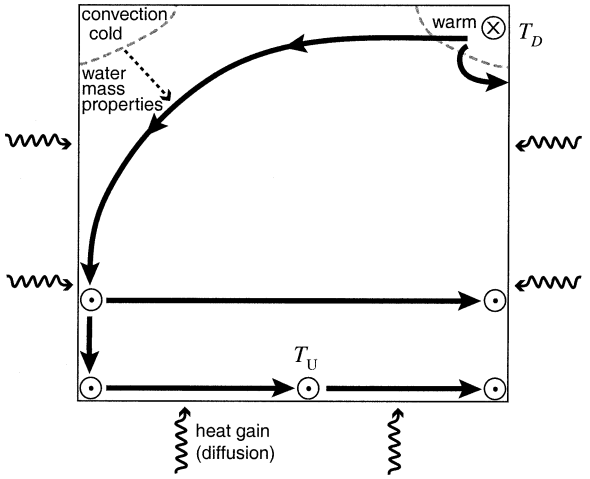

FIG. 12. Illustration (plan view) of abyssal flow and heat budget. Flow downwells (as indicated by the circled ''×'') in the northeast corner at temperature T_D and its water mass properties are subsequently modified as it flows adjacent to deep convection in the northwest. Flow then proceeds along the western boundary; some flow upwells (as indicated by the circled ''•'') in the western boundary, some flow reaches the equator and upwells, and some flow moves across the basin before upwelling in the east. Downward diffusion of heat along the boundaries is balanced by upwelling so that the flow is warmed slightly in low latitudes, upwelling at average temperature T_U.

site of deep convection is anomalously cold, the geostrophic flow is around rather than through this region, so horizontal advection is also ineffective at conveying its water mass properties. Rather, this cold water is spread through the deep ocean by mesoscale eddy transfers, here represented by the Gent and McWilliams (1990) parameterization. One way to quantify this effect is via a ''bolus'' downwelling at the deep convection site and a bolus upwelling in the warmer sectors of the deep ocean. Thus, both deep downwelling and deep convection play a role in determining abyssal water mass properties (see also Marotzke and Scott 1999; Huck et al. 1999).

The relatively minor role played by abyssal mixing in setting MOC strength through the thermocline stands in marked contrast to other recent discussions (e.g., MW; Ledwell et al. 2000), so a careful analysis of the abyssal heat budget is warranted. To reconcile the abyssal heat budget, consider the signs of the relevant flux terms. Let us first consider the mixing processes. In steady state, convective mixing causes a heat loss, and diffusion produces a heat gain. In our control boundary mixing run, however, the contribution from both of these sources is small. Given that deep flow is around rather than through the site of deep convection, scant heat is convectively mixed out of the abyss. The heat gain from diffusion is also small due to the model's weak stratification in the abyss.

The vertical advective heat gain in the abyss is proportional to the following expression:

$$\int wT\, dA = \int_{\text{downwelling}} w_D T_D + \int_{\text{upwelling}} w_U T_U, \quad (6)$$

where the U and D subscripts refer to upwelling and downwelling, respectively. This term seemingly could be positive or negative, but we suggest it must yield a heat gain (i.e., $T_D > T_U$, and by continuity $-w_D = w_U$), unless there are other deep diabatic sources/sinks such as geothermal heating (Scott et al. 2001). The advective heat gain is largely balanced by the remaining term in the budget, namely a heat loss from the parameterization of mesoscale eddies along isopycnals, which leads to a bolus heat transport opposite that of the advective transport.

For a more quantitative justification of these results, we made some rough calculations of the heat fluxes into the upper and lower aybss. In the lower abyss (bottom 1000 m), the diffusive heat flux $\rho c_p \kappa \partial_z T$ is of order 0.1 TW, whereas the larger balance is between heating via advection and cooling through bolus transport, with terms on the order of 1 TW. Thus, despite the vertical balance in the Tropics (i.e., where mixing occurs) being advective–diffusive, the diffusive heat flux is a lower order term in the full balance. In the upper abyss, the stratification increases by an order of magnitude (and therefore the diffusive heat transport increases), but both the advective heating and bolus transport cooling also increase, due to both an increased magnitude of flow and an increased disparity between T_U and T_D. In the thermocline, the balance among these heat fluxes is quite different, particularly the top 500 m. Here, the diffusive flux is quite large, approximately 0.5 PW (i.e., the magnitude of the equator-to-pole heat flux), whereas both advection and bolus transport contribute a upward flux, but less than 0.1 PW. Presumably, the balancing upward heat flux is by convection in (deep) mixed layers.

The insensitivity of the overturning maximum to deep mixing, as would be suggested by our numerical results, is consistent with our observation that diffusive heating is not a dominant term in the abyssal heat budget. On the other hand, the differences in flow through the abyss as shown in Figs. 10a and 10b imply that the strength of deep mixing affects the density structure of the deep ocean. Figures 13a and 14a show the temperature and stratification ($\partial T/\partial z$) at the west and east sides of the equator, respectively, for the depth-dependent mixing runs. With strong deep mixing, the bottom water is slightly warmer in low latitudes, that is, the tail end of the abyssal flow pathway, consistent with a larger diffusive heat flux to the bottom. Similarly, weaker diffusive fluxes leads to colder bottom water at low latitudes. The temperature at the deep convection site, which is linked to the coldest surface temperature, is little changed in both cases (not shown).

Surprisingly, the low-latitude abyss is less stratified in both the weak and strong mixing cases. With weak deep mixing, less heat is diffused downward, whereas

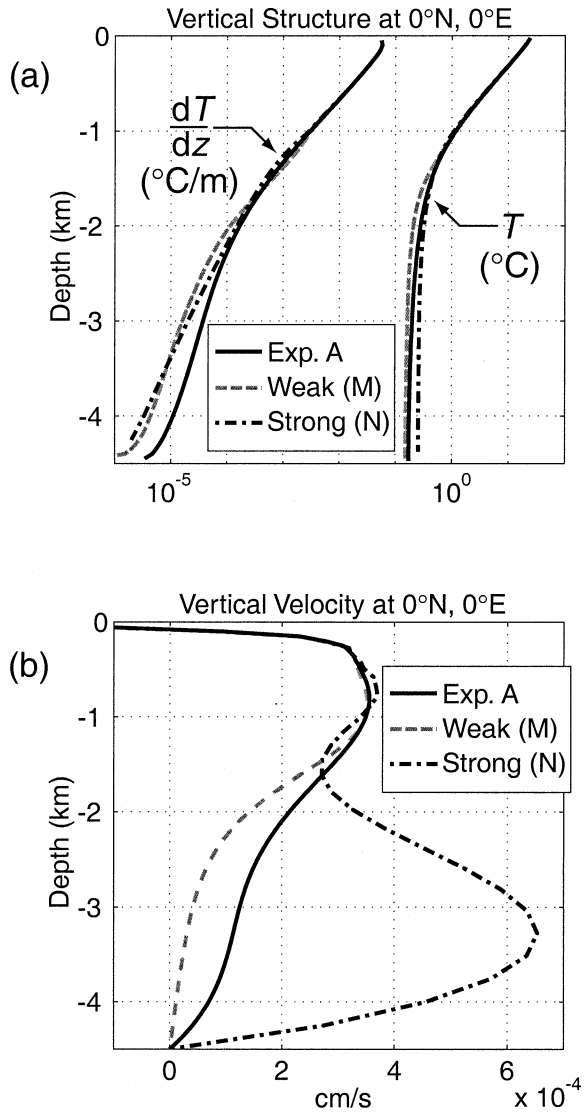

FIG. 13. (a) Vertical potential temperature structure and (b) vertical velocity at the western extreme of the equator for the control boundary mixing (expt A), weak deep mixing (expt M), and strong deep mixing run (expt N).

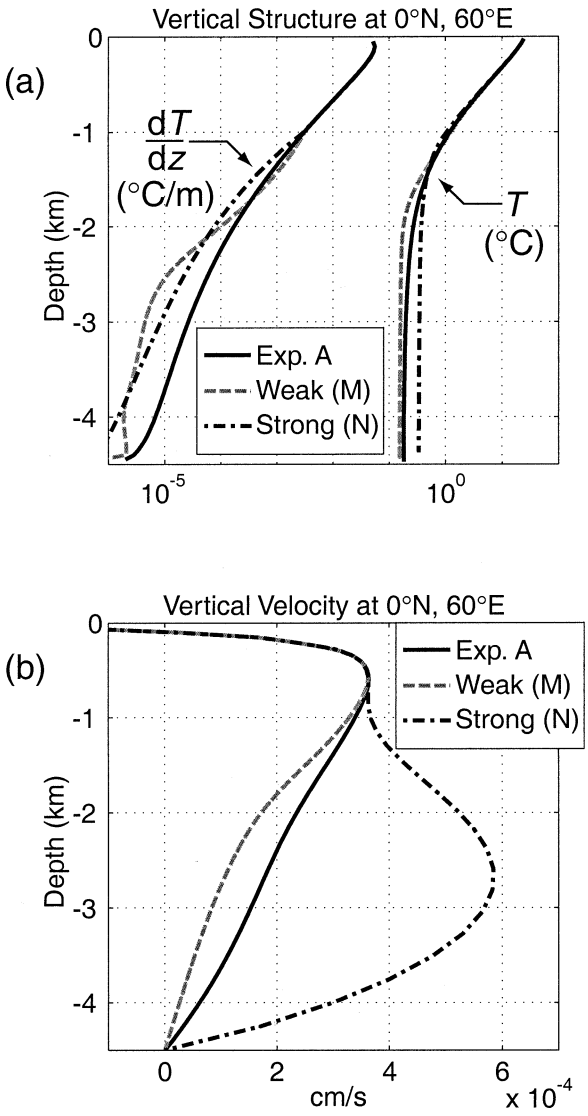

FIG. 14. (a) Vertical potential temperature structure and (b) vertical velocity at the eastern extreme of the equator for the control boundary mixing (expt A), weak deep mixing (expt M), and strong deep mixing run (expt N).

in the strong mixing case diffusion is so efficient at mixing heat that the temperature gradient is degraded. This latter result is in contrast with CHG and Cummins (1991), where stronger stratification with increased deep mixing was observed. However, when we scaled back the increase in deep mixing so that the area-weighted diffusivity at each vertical level was more similar to that in Cummins (expt O), we too observed increased stratification at depth (not shown). More specifically, the deep ocean stratification doubled, although stratification in the 1000 m below the thermocline was weaker. We speculate that some ''optimum'' profile of κ could lead to a maximum stratification at depth, although further research along these lines is beyond the scope of this paper.

As suggested by the plots of meridional overturning streamfunction, upwelling at the equator varies considerably between deep mixing runs (Figs. 13b and 14b). A weaker diffusive flux requires less upwelling for steady-state balance, and therefore it is no longer necessary for such a large percentage of abyssal upwelling to occur at the equator. Conversely, in the strong deep mixing case the larger equatorial diffusive heat flux must be balanced by strong upwelling. Without sufficient mixing in the thermocline, however, this upwelling essentially ''detrains'' from the larger cell, flowing horizontally and downward away from the equator.

Our analysis of the abyssal heat budget also suggests an explanation for the differences in the behavior on the east and west (cf. Fig. 13 vs Fig. 14). Because the abys-

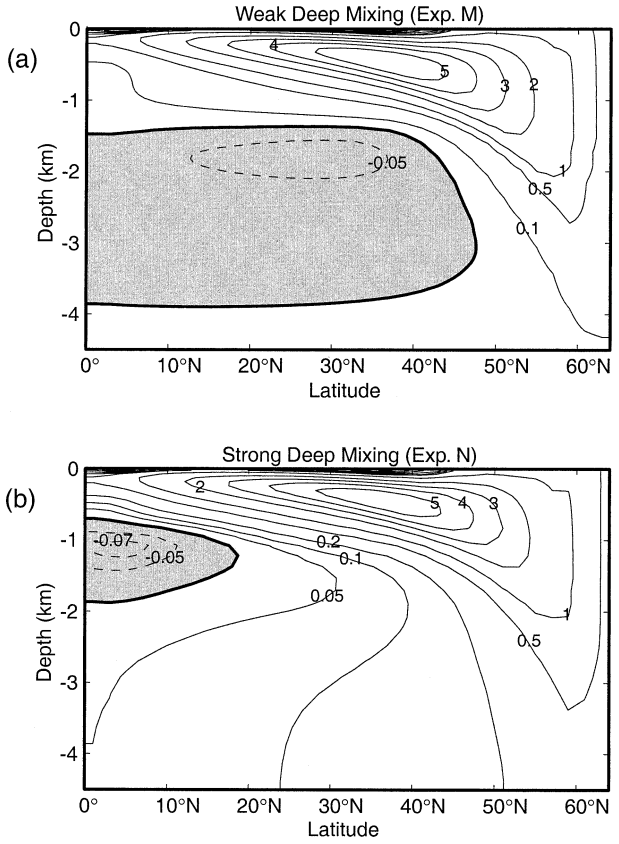

FIG. 15. Potential temperature difference between the eastern and western boundary for (a) weak deep mixing (expt M) and (b) strong deep mixing run (expt N). The difference is negative in shaded areas.

sal flow reaches the western boundary soon after downwelling, diffusion has had less time to alter the stratification. Thus, the stratification in the west is less affected by the magnitude of deep mixing. In contrast, in the east the ocean is virtually unstratified in the bottom 2000 m in the weak mixing run, and stratification also falls off more sharply (as compared with the control run) in the strong mixing case.

Differences in the upwelling profile are consistent with thermal wind balance of the zonally averaged deep overturning circulation. More specifically, note that the western boundary upwelling in the weak deep mixing run is sharply reduced. As a result, some heat penetrates downward on the west (mixing may be weak, but is still nonzero), so the nearly unstratified eastern boundary is colder than the west throughout much of the abyss (Fig. 15a). The resulting east–west temperature difference is such that zonally averaged southward flow increases from the bottom upward, consistent with the overturning pattern observed in Fig. 10a. In the strong deep mixing run, upwelling on the eastern boundary peaks higher in the water column as compared to the west, which in turn produces a dipole pattern east–west temperature difference at depth (Fig. 15b). The warmer eastern boundary near the bottom is necessary to support the shear required for the deep equatorial overturning cell, but the east must also be colder near the base of the thermocline in order to attenuate the northward flow associated with the top of this cell.

5. Discussion

We have presented a series of numerical experiments that explore the large-scale consequences of mixing location. Our single-hemisphere model is highly idealized, lacking wind forcing and topography, although we submit that our results provide context for speculation about the dynamics of the real ocean.

Given the different processes thought to play a role in the steady state balance of the MOC—convection, rotation, and buoyancy forcing—it is not directly apparent why the strength of the MOC is a function of the magnitude and distribution of diapycnal diffusivity. According to ''Sandström's theorem'' (Sandström 1908), given surface heating at a higher geopotential than cooling (neglecting the smaller geothermal heat fluxes at the ocean floor), the steady-state ocean circulation should, for all intents and purposes, be motionless except in a thin upper layer. In other words, given heating in the Tropics, the ocean should not be able to operate as a heat engine, extracting energy from the surface buoyancy forcing to maintain a strong MOC. However, Jeffreys (1925) argued that turbulent mixing could effectively lower the geopotential of heating, leading to horizontal temperature gradients at depth which would in turn lead to a vigorous circulation [see Colin de Verdière (1993), MW, and Huang (1999) for a more thorough discussion of Sandström's theorem and the controversy surrounding its application to the ocean].

In the model, we find that diapycnal (nonconvective) mixing at mid and high latitudes is not critical in order to generate a MOC, given that surface temperatures there are relatively low and hence diffusive heat fluxes are much weaker than in the Tropics. Mixing at low latitudes, where the surface temperature is high, is more efficient at diffusing heat beneath the mixed layer and hence more effective at driving the MOC. This result suggests that thermodynamic considerations of the ocean circulation are indeed fundamental: The strength of the MOC is a direct function of the surface heat input that diffuses into the thermocline. Diapycnal mixing in the tropical thermocline communicates the surface buoyancy fluxes into the interior, which in turn increases potential energy. In conjunction with convective mixing at high latitudes, the penetration of heat leads to horizontal temperature gradients beneath the surface. In geostrophic balance, these temperature gradients generate strong zonal flows into the eastern boundary that subsequently downwell, leading to an east–west temperature difference that provides the vertical shear necessary for the MOC (Zhang et al. 1992; Colin de Verdière 1993; Marotzke 1997).

Comparison of boundary mixing with interior mixing

indicates that planetary geostrophic vorticity balance in the interior, the cornerstone of the Stommel and Arons (1960) theory for the abyssal component of the large-scale overturning circulation, actually hinders the process leading to east–west density differences, which can support the MOC through thermal wind shear. As required by conservation of planetary vorticity, vortex stretching or compression in the ocean interior is accompanied by meridional flow. Here, we find that vortex compression in the thermocline effectively restricts the communication of warm waters to the eastern boundary, and therefore interior mixing is less effective at driving a vigorous MOC than boundary mixing. With boundary mixing, where frictional effects enter the vorticity balance, heat penetration into the thermocline leads to stronger zonal flows that downwell to greater depth at the eastern boundary.

Our model results suggest that deep downwelling waters are relatively buoyant, and to lowest order the abyssal heat balance is between advective transport (producing a heat gain) and cooling through the effect of mesoscale eddies along isopycnals, here represented by the Gent and McWilliams (1990) parameterization. Thus, the abyssal water mass properties are an average of the properties tied to deep convection and that of deep mass injection. The magnitude of deep mixing can affect the bottom water temperature, however. With very weak mixing, the abyss is colder and nearly homogeneous, and flow upwells quasi-adiabatically into the thermocline. Stronger mixing produces a warmer abyss and dictates that upwelling in the abyss occurs diabatically, where mixing is located. An interesting corollary is that the temperature at the base of the thermocline appears to be set by the temperature of the downwelling water (see Fig. 2b).

Observed stratification of the real abyss might suggest the presence of enhanced deep mixing there. Dissipation of tides is thought to produce elevated mixing at depth near rough bottom topography (Polzin et al. 1997), and also several 100 m above, presumably through upward internal wave propagation. An idea expressed in MW is that diapycnal mixing in the abyss, resulting from the energy input of winds and tides, is fundamentally necessary to return deep waters back into the thermocline. Our results suggest that this enhanced deep mixing by itself is insufficient to support a strong MOC and heat transport, and has little effect on the strength of the circulation through the thermocline; rather, elevated mixing must be found at thermocline depths. A corollary of this result is that abyssal mixing is not necessary for a vigorous deep circulation (i.e., mixing in the thermocline is sufficient). Recent microstructure measurements off Cape Hatteras indicate strong mixing at thermocline depths above rough bottom topography, although of very limited spatial extent and primarily confined to depths below 500 m (K. Polzin 2002, personal communication). Similar measurements in the Gulf Stream, above gently sloping terrain, suggest only slightly elevated levels of mixing. Only very recently have significant areas of elevated mixing in the thermocline been located, in the salt-fingering area of the western subtropical North Atlantic (R. Schmitt 2002, personal communication).

In the real ocean, mixing at depth may play an additional role, which is not addressed here, namely its capacity to homogenize water masses of different origin (e.g., North Atlantic Deep Water and Antarctic Bottom Water). Our results show that the deep circulation pattern induced by deep mixing (or lack thereof) is confined below the thermocline and does not transport any significant amount of heat, and therefore does not play a significant role in determining the oceanic meridional heat transport. Although the bottom-water temperature is affected by the deep mixing, we suggest that this has only minor impact on the meridional heat flux, in contrast with the argument put forth in Cummins et al. (1991) to explain this insensitivity. The maximum in the overturning streamfunction may be affected by deep mixing through superposition of the deep circulation with the surface-forced overturning, depending on the vertical profile of mixing in the abyss.

In part due to the lack of observed thermocline mixing, other ideas regarding the importance of the Southern Hemisphere in driving North Atlantic Deep Water production have recently been gaining favor. One possibility is that the winds over the Antarctic Circumpolar Channel (ACC) lead to enhanced mixing there, as discussed in Wunsch (1998). Using a general circulation model of an idealized ocean basin, Marotzke and Klinger (2000) found increased cross-equatorial transport with enhanced mixing in the Southern Hemisphere, consistent with our results that show upwelling occurs where mixing is located. However, if mixing is concentrated in the latitude band of the ACC, our model results suggest that this would not be effective in driving a strong MOC, as the cool surface temperatures would lead to weak diffusive heat flux penetrating into the thermocline.

A second variation on the role of the Southern Ocean is that the wind stress over the ACC produces a ''Drake Passage effect'' whereby these winds induce a northward Ekman transport that can only return southward geostrophically below the sill of Drake Passage, hence requiring its transformation into North Atlantic Deep Water (Toggweiler and Samuels 1995). The flow is subsequently returned to the surface though Ekman suction in Drake Passage. In coarse-resolution general circulation models, a nearly linearly relation between northern deep-water production and Southern Hemisphere winds has been observed (McDermott 1996), perhaps obviating the need for any significant sources of mixing in order to produce a vigorous overturning circulation (Toggweiler and Samuels 1998). Again, we caution the direct applicability of our idealized model to the real ocean, in as much as we do not have any wind-induced upwelling, nor does our model do justice when it comes

to representing the complexity of the oceans' water mass properties. Although model results show that the presence of the channel can lead to increased thermocline depth (e.g., Gill and Bryan 1971; Vallis 2000), the thermodynamic considerations we have examined suggest that it must be investigated *how* this mechanism leads to the east–west temperature differences necessary to support a pole-to-pole overturning cell in thermal wind balance.

Our standard boundary mixing is parameterized in vertical columns many kilometers wide, which provides an equal area of mixing at all depths. In the real ocean, the boundaries are more horizontal than vertical, and mixing likely occurs over a significantly reduced length scale normal to the boundary. Moreover, the effect of diapycnal mixing on sloping boundary has been shown to have dynamical consequences (Garrett 1991, 2001; Thompson and Johnson 1996), which may influence the large-scale circulation. The presence of sloping boundaries at high latitudes affects the volume of deep mass transport by requiring deep convection to occur in the open ocean (Spall and Pickart 2001), which may alter our depiction of the abyssal heat balance.

6. Conclusions

The main conclusions from our idealized model experiments are as follows.

1) Boundary mixing is more efficient than interior mixing in causing a strong MOC.
2) The MOC strength through the thermocline, and the associated heat transport, are mainly determined by thermocline mixing at low latitudes, where the vertical temperature gradient is strong. In contrast, high-latitude and deep mixing play lesser roles.
3) Mixing plays a minor role in the deep-ocean heat budget.

Acknowledgments. The authors thank Carl Wunsch, Kerry Emanuel, Barry Klinger, Peter Stone, and Hua Ru for discussions and comments on an earlier version of this manuscript. The anonymous reviewers significantly contributed to improving the paper. JS was supported by the MIT Joint Program on the Science and Policy of Global Change and by the U.S. Department of Energy's Office of Biological and Environmental Research Grant DE-FG02-93ER61677. JM was supported by NSF Grant 9810800.

REFERENCES

Bryan, F., 1987: Parameter sensitivity of primitive equation ocean general circulation models. *J. Phys. Oceanogr.,* **17,** 970–985.
——, and M. Cox, 1967: A numerical investigation of the oceanic general circulation. *Tellus,* **19,** 54–80.
Colin de Verdière, A., 1988: Buoyancy driven planetary flows. *J. Mar. Res.,* **46,** 215–265.
——, 1993: On the oceanic thermohaline circulation. *Modelling Oceanic Climate Interactions*, J. Willebrand and D. L. T. Anderson, Eds., NATO ASI Series, Springer, 151–183.
Cummins, P., 1991: The deep water stratification of ocean general circulation models. *Atmos.–Ocean,* **19,** 563–575.
——, G. Holloway, and A. E. Gargett, 1990: Sensitivity of the GFDL ocean general circulation model to a parameterization of vertical diffusion. *J. Phys. Oceanogr.,* **20,** 817–830.
Garrett, C., 1991: Marginal mixing theories. *Atmos.–Ocean,* **29,** 313–339.
——, 2001: An isopycual view of near-boundary mixing and associated flows. *J. Phys. Oceanogr.,* **31,** 138–142.
Gent, P. R. and J. C. McWilliams, 1990: *J. Phys. Oceanogr.,* **20,** 150–155.
Gerdes, R. C., C. Köberle, and J. Willebrand, 1991: The influence of numerical advection schemes on the results of ocean general circulation models. *Climate Dyn.,* **5,** 211–226.
Gill, A. E., 1982: *Atmosphere–Ocean Dynamics.* Academic Press, 662 pp.
——, and K. Bryan, 1971: Effects of geometry on the circulation of a three-dimensional southern-hemisphere ocean model. *Deep-Sea Res.,* **18,** 685–721.
Gregg, M. C., 1987: Diapycnal mixing in the thermocline: A review. *J. Geophys. Res.,* **92,** 5249–5286.
Griffies, S. M., A. Gnanadesikan, R. C. Pacanowski, V. D. Larichev, J. K. Dukowicz, and R. D. Smith, 1998: Isoneutral diffusion in a *z*-coordinate ocean model. *J. Phys. Oceanogr.,* **28,** 805–830.
Hasumi, H., and N. Suginohara, 1999: Effects of locally enhanced vertical diffusivity over rough bathymetry on the world ocean circulation. *J. Geophys. Res.,* **104,** 23 367–23 374.
Huang, R. X., 1999: Mixing and energetics of the oceanic thermohaline circulation. *J. Phys. Oceanogr.,* **29,** 727–746.
Huck, T., A. J. Weaver, and A. Colin de Verdière, 1999: On the influence of the parameterization of lateral boundary layers on the thermohaline circulation in coarse-resolution ocean models. *J. Mar. Res.,* **57,** 387–426.
Jeffreys, H., 1925: On fluid motions produced by differences of temperature and humidity. *Quart. J. Roy. Meteor. Soc.,* **51,** 347–356.
Ledwell, J. R., A. J. Watson, and C. S. Law, 1993: Evidence for slow mixing across the pycnocline from an open-ocean tracer release experiment. *Nature,* **364,** 701–703.
——, E. T. Montgomery, K. L. Polzin, L. C. St. Laurent, R. W. Schmitt, and J. M. Toole, 2000: Evidence for enhanced mixing over rough topography in the abyssal ocean. *Nature,* **403,** 179–182.
Marotzke, J., 1997: Boundary mixing and the dynamics of three-dimensional thermohaline circulations. *J. Phys. Oceanogr.,* **27,** 1713–1728.
——, and J. R. Scott, 1999: Convective mixing and the thermohaline circulation. *J. Phys. Oceanogr.,* **29,** 2962–2970.
——, and B. A. Klinger, 2000: The dynamics of equatorially asymmetric thermohaline circulations. *J. Phys. Oceanogr.,* **30,** 955–970.
McDermott, D. A., 1996: The regulation of northern overturning by Southern Hemisphere winds. *J. Phys. Oceanogr.,* **26,** 1234–1255.
Munk, W., 1966: Abyssal recipes. *Deep-Sea Res.,* **13,** 707–730.
——, and C. Wunsch, 1998: Abyssal recipes II: Energetics of tidal and wind mixing. *Deep-Sea Res.,* **45,** 1977–2010.
Pacanowski, R. C., 1996: MOM 2.0 documentation, user's guide, and reference manual. GFDL Ocean Tech. Rep. 3.1, NOAA/Geophysical Fluid Dynamics Laboratory, Princeton, NJ. [Available from NOAA/GFDL, Princeton University, P.O. Box 308, Princeton, NJ 08542.]
Park, Y.-G., and K. Bryan, 2000: Comparison of thermally driven circulations from a depth-coordinate model and an isopycnal-layer mode. Part. I: A scaling-law sensitivity to vertical diffusivity. *J. Phys. Oceanogr.,* **30,** 590–605.
Pedlosky, J., 1996: *Ocean Circulation Theory.* Springer, 453 pp.
Peters, H., M. C. Gregg, and J. M. Toole, 1988: On the parameter-

ization of equatorial turbulence. *J. Geophys. Res.*, **93,** 1199–1218.
Polzin, K. L., J. M. Toole, J. R. Ledwell, and R. W. Schmitt, 1997: Spatial variability of turbulent mixing in the abyssal ocean. *Science*, **276,** 93–96.
Redi, M. H., 1982: Oceanic isopycnal mixing by coordinate rotation. *J. Phys. Oceanogr.*, **12,** 1154–1158.
Samelson, R. M., 1998: Large-scale circulation with locally enhanced vertical mixing. *J. Phys. Oceanogr.*, **28,** 712–726.
Sandström, J. W., 1908: Dynamische Versuche mit Meerwasser. *Ann. Hydrographie Marit. Meteor.*, **36,** 6–36.
Scott, J. R., 2000: The roles of mixing, geothermal heating, and surface buoyancy forcing in ocean meridional overturning dynamics. Ph.D. thesis, Massachusetts Institute of Technology, 128 pp.
——, J. Marotzke, and A. Adcroft, 2001: Geothermal heating and its influence on the meridional overturning circulation. *J. Geophys. Res.*, **106,** 31 141–31 154.
Spall, M. A., 2000: Large-scale circulations forced by mixing near boundaries. *J. Mar. Res.*, **58,** 957–982.
——, and R. S. Pickart, 2001: Where does dense water sink? A subpolar gyre example. *J. Phys. Oceanogr.*, **31,** 810–826.
Stommel, H., 1982: Is the South Pacific helium-3 plume dynamically active? *Earth Planet Sci. Lett.*, **61,** 63–67.
——, and A. B. Arons, 1960: On the abyssal circulation of the world ocean—I. Stationary planetary flow patterns on a sphere. *Deep-Sea Res.*, **6,** 140–154.
Thompson, L., and G. C. Johnson, 1996: Abyssal currents generated by diffusion and geothermal heating over rises. *Deep-Sea Res.*, **43,** 193–211.
Toggweiler, J. R., and B. Samuels, 1995: Effect of Drake Passage on the global thermohaline circulation. *Deep-Sea Res.*, **42,** 477–500.
——, and ——, 1998: On the ocean's large-scale circulation near the limit of no vertical mixing. *J. Phys. Oceanogr.*, **28,** 1832–1852.
Vallis, G. K., 2000: Large-scale circulation and production of stratification: Effects of wind, geometry, and diffusion. *J. Phys. Oceanogr.*, **30,** 933–954.
Veronis, G., 1975: The role of models in tracer studies. *Numerical Models of the Ocean Circulation*, Natl. Acad. Sci., 133–146.
Welander, P., 1971: The thermocline problem. *Philos. Trans. Roy. Soc. London*, **A270,** 415–421.
Winton, M., 1993: Numerical investigations of steady and oscillating thermohaline circulations. Ph.D. thesis, University of Washington, 155 pp.
Wunsch, C., 1998: The work done by the wind on the ocean circulation. *J. Phys. Oceanogr.*, **28,** 2331–2339.
Zhang, J., R. W. Schmitt, and R. X. Huang, 1999: The relative influence of diapycnal mixing and hydrologic forcing on the stability of the thermohaline circulation. *J. Phys. Oceanogr.*, **29,** 1096–1108.
Zhang, S., C. A. Lin, and R. J. Greatbatch, 1992: A thermocline model for ocean-climate studies. *J. Mar. Res.*, **50,** 99–124.